Modeling and Simulation of Convection-Dominated Species Transport in the Vicinity of Rising Bubbles

Andre Weiner and Dieter Bothe

Abstract For multiphase contactors, like bubble column reactors, it is of highest interest to predict how the gas dissolves and reacts in the liquid phase. This mass transfer process strongly depends on convection-dominated, extremely thin species boundary layers forming at the liquid-side of the bubble's surface. Numerical simulations can play a significant role in understanding and predicting the complex interactions between flow dynamics and species transport, but the direct solution of both phenomena at the same time is currently not possible. This chapter summarizes two approximation approaches for the efficient and accurate simulation of convection-dominated concentration boundary layers. The first approach is a subgrid-scale model which allows to handle boundary layer widths that can be far smaller than the first cell layer at the interface in the computational mesh. Convective fluxes, diffusive fluxes and reaction source terms in the finite volume method are corrected based on non-linear reconstructions of the species boundary layer profiles normal to the interface. The second method is a hybrid simulation approach that solves the two-phase flow problem based on the Volume-of-Fluid method and uses a single-phase solver for species transport simulations. The concentration boundary layer is computed using a highly resolved surface-aligned single phase mesh.

1 Introduction

Bubbly flows in bubble column reactors exhibit a large range of bubble sizes undergoing topological due to break-up or coalescence. However, state-of-the-art numerical methods for interface-resolved simulations struggle already with much simpler settings due to enormous computational costs. A millimeter-sized bubble rising in water at room temperature reaches a terminal velocity of approximately $v = 0.25$ m/s. Assuming a kinematic liquid viscosity of $\nu = 10^{-6}$ m^2/s yields a Reynolds number of

A. Weiner · D. Bothe (✉)
Technical University of Darmstadt, Mathematical Modeling and Analysis, Alarich-Weiss-Str. 10, 64287 Darmstadt, Germany
e-mail: bothe@mma.tu-darmstadt.de

M. Schlüter et al. (eds.), *Reactive Bubbly Flows*, Fluid Mechanics and Its Applications 128, https://doi.org/10.1007/978-3-030-72361-3_14

$$Re = \frac{d_b U_b}{\nu_l} = \frac{0.001 \times 0.25}{10^{-6}} = 250. \tag{1}$$

In the absence of surface active agents or contaminants, the gas-liquid interface may be considered as fully mobile. The shear forces at the bubble surface are small compared to, for example, the ones acting at the solid-liquid interface of a rising particle. As a consequence, only a small layer of liquid is significantly set in motion around a rising bubble. The wake region may be considered an exception to this observation in some cases. The thickness of the flow boundary layer δ_h around a nearly spherical rising bubble can be estimated using the relation

$$\delta_h = \frac{d_b}{\sqrt{2\,Re}}. \tag{2}$$

We refer to page 263 in Ref. [1] for more details. Also for non-spherical bubble shapes, the scaling often follows the relation $\delta_h \propto d_b/\sqrt{Re}$. Coming back to the example of a millimeter-sized bubble, the average flow boundary layer width is roughly fifteen times smaller than the bubble diameter.

The transport of chemical species within the liquid bulk occurs on smaller length scales compared to the transport of momentum. The ratio of the length scales is often characterized by means of the Schmidt number $Sc = \nu_l/D$, where D stands for the molecular diffusivity of a chemical species dissolved in the liquid phase. As an example, the Schmidt number for oxygen dissolved in water at room temperature is about 400. The ratio between species and flow boundary layer at a clean gas-liquid interface follows the trend $\delta_c \propto \delta_h/\sqrt{Sc}$. Considering a millimeter-sized oxygen bubble and the previous specimen calculation for the flow boundary layer, it can be stated that the average species boundary layer width is roughly twenty times smaller than its flow counterpart, and that it is even 300 times smaller than the bubble size. The latter fact may be also expressed more directly using the Péclet number $Pe = Re\,Sc$ and the scaling $\delta_c \propto d_b/\sqrt{Pe}$.

The consequence of this large gap between bubble size and boundary layer thickness can be experienced firsthand by looking at Fig. 1. An oxygen bubble moves in a confined channel and forms a Taylor bubble. The gaseous oxygen dissolves and reacts with a copper complex present in the liquid phase. The reaction product

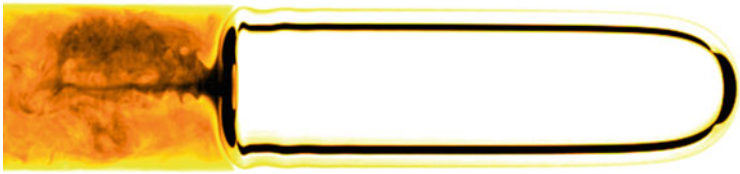

Fig. 1 Oxygen bubble moving (from left to right) in a channel filled with water. The oxygen dissolves and reacts with a copper complex present in the water phase yielding a brownish color. Picture from www.dfg-spp1740.com

displays a yellow-brown color. Looking at the picture, it appears that most of the oxygen is dissolved at the bottom of the bubble (the left end in Fig. 1). What actually happens is that the oxygen dissolves over the entire surface of the bubble while being transported in an extremely thin layer to the rear part of the bubble. Only when the flow detaches from the interface, the reaction product becomes visually accessible in the bubble wake.

The problem of thin boundary layers or, in terms of dimensionless numbers, high Schmidt and Péclet numbers poses an enormous challenge for both experimental and numerical means of investigation. The mass transfer rate, but also yield and conversion in the presence of a chemical reaction are to a large extend determined by the species boundary layers. It goes without saying that investigations are even more challenging if chemical reactions take place and multiple species have to be considered.

The only class of numerical approaches that is currently able to approximate species transfer at rising bubbles for realistic Péclet numbers relies on subgrid-scale (SGS) modeling. There are currently two branches of such subgrid-scale models available in the literature. The first model type was designed for Front-Tracking based two-phase flow solvers [2–4] and completely omits the numerical solution of the species transport equation on the Eulerian grid in a defined narrow region around the interface. Instead, each front marker point carries an additional scalar value representing the amount of species in the boundary layer in its vicinity. The boundary layer mass is updated each time step by reconstructing and evaluating the species distribution in interface normal direction. Once the boundary layer mass of a marker point exceeds a certain threshold, the species is released into the liquid bulk. The approach is relatively simple but very effective in terms of accuracy. A drawback is that it is currently not clear how to incorporate two-sided interactions between boundary layer and liquid bulk. Recent approaches only release species into the liquid bulk but ignore the ambient bulk concentration.

The second class of subgrid-scale models was developed for finite volume solvers and reconstructs the concentration profile in interface normal direction based on the liquid-side concentration in an interfacial cell [5–11]. The reconstructed profile is then used to correct the face-fluxes in the typical finite volume discretization of convection and diffusion terms. In the context of two-phase approaches this correction mechanism has been implemented in Volume-of-Fluid [5, 6, 9] and Interface-Tracking [7, 11] approaches. Since the profile reconstruction is based on concentration values close to the interface, changes in the liquid bulk concentration are naturally included. However, this advantage comes at the cost of increased algorithmic complexity or restricted mesh topology support close to the gas-liquid interface.

This chapter summarizes recent developments in the flux-based subgrid-scale modeling approach [8–10]. These developments concern the profile reconstruction, the flux correction, the extension to multiple species and reactions, and the validation of new models.

2 Numerical Methods

2.1 Geometrical Volume-of-Fluid Approach

The results presented in the following sections have been obtained with two Volume-of-Fluid based solvers, namely Free Surface 3D[1] (FS3D) [5, 6, 9] and Basilisk[2]; we refer to the literature cited in Chap. 3.1 of [8] for more information on Basilisk. Both solvers transport the volume fraction field using geometrically calculated fluxes. Also the curvature computation, needed for the application of surface tension forces, relies on height functions in both approaches. The main differences between the solvers relates to two important features: adaptive mesh refinement and the two-scalar approach for species transport.

The concentration jump of chemical species at the gas-liquid interface poses a severe difficulty for numerical modeling. The two-scalar approach implemented in FS3D [5] overcomes this challenge by introducing two distinct scalar fields for each chemical species: one for the liquid and one for the gas phase. Both fields are connected via mass-exchange terms in interface cells. Moreover, convective species fluxes in interface cells rely in the geometrically computed fluxes for the volume-fraction transport. Therefore, no artificial mass transfer due to erroneous convective fluxes takes place. The two-scalar approach requires more memory than, for example, the single-field approach, but the numerical solution of the species transport is characterized by a comparatively high accuracy, especially in the interface vicinity.

The computational mesh in FS3D consist always of one or more structured Cartesian blocks. Structured meshes allow efficient computations and enable simplified implementation and testing of new algorithms. Such meshes are also favorable when a uniformly high resolution is required and the spatial scales vary over less than three to four orders of magnitude. In the field of bubbly flows, the uniform resolutions practically limits simulations to Reynolds numbers below roughly 500 and moderate shape deformations. Currently, it is not feasible to simulate the flow dynamics of characteristic bubble shapes like spherical cap or dimpled ellipsoidal.

The range of investigated scales can be increased by means of numerical techniques like adaptive mesh refinement, as employed in the Basilisk-based flow solver; see Fig. 2. The mesh resolution is adapted locally according to the flow features in the simulation. The results presented in the following sections were obtained using a so-called wavelet refinement. The mesh adaptation algorithm works as follows: first, the solution on the current grid is mapped to the next coarsest refinement level by an averaging process. Then, the fine grid solution is reconstructed from the mapped field. The discrepancy between the up-sampled and the actual field is used as an error estimator and can be compared against a fixed user-defined criterion. If the accuracy loss due to down-sampling is higher than the given threshold, the grid is

[1] www.mma.tu-darmstadt.de.

[2] www.basilisk.fr.

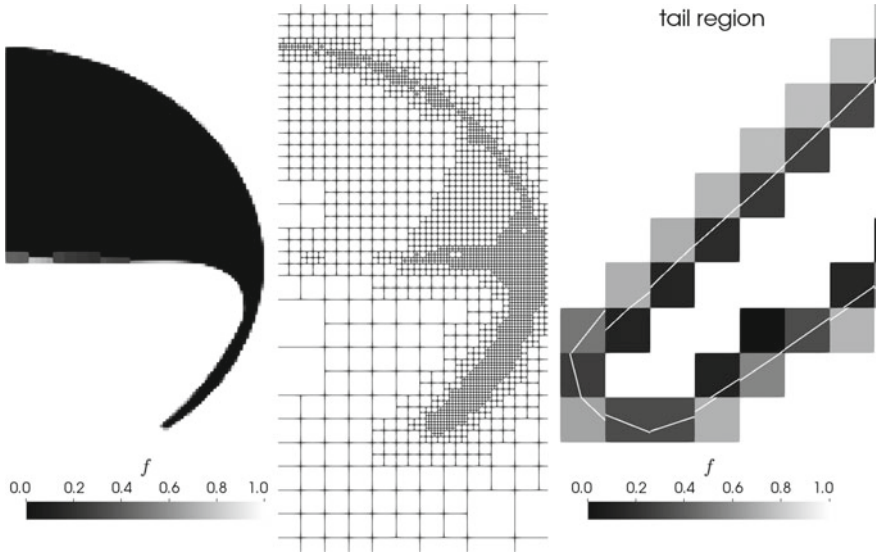

Fig. 2 Typical elements of a Volume-of-Fluid simulation in Basilisk (www.basilisk.fr). Volume fraction field (left), adaptively refined background mesh (center), and reconstructed interface elements (right)

refined. If the information loss is marginal, the grid is coarsened. The refinement and un-refinement operations are limited by a prescribed lower and upper bound of the allowed refinement level.

A drawback of two-phase flow solver implemented in Basilisk is that the two-scalar approach for species transport is currently not implemented. Therefore, the following chapters present results obtained with FS3D as well as with Basilisk.

2.2 Single-Phase Approximation

The single-phase approximation or hybrid approach was developed due to a lack of available reference data for subgrid-scale model validation. The idea is to combine the robustness and efficiency of Volume-of-Fluid simulations with the accuracy of surface aligned unstructured meshes. The combination of these favorable attributes happens in three steps:

1. A two-phase Volume-of-Fluid simulation, as described in the previous section, is executed to obtain the bubble rise velocity, the interface deformation, and the velocity vector at the gas liquid interface.
2. An explicit representation of the bubble shape is created based on the volume fraction field and saved as a geometry file; see Fig. 3.

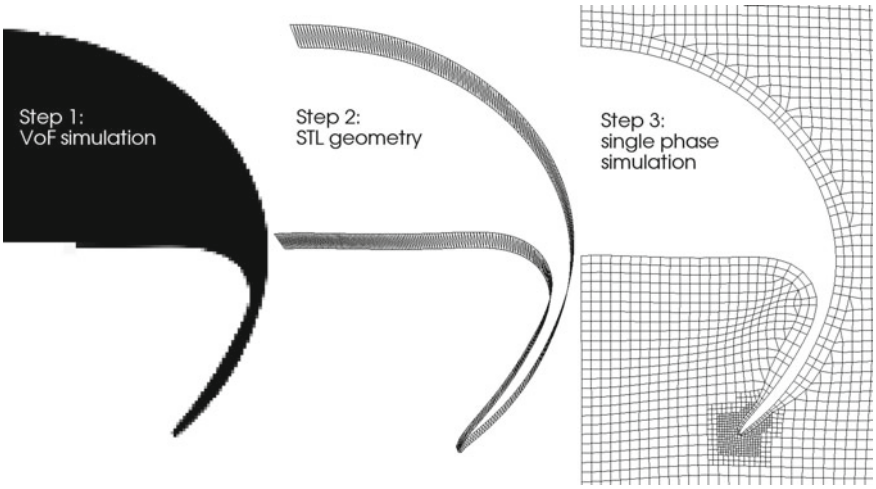

Fig. 3 Three essential steps in the single phase approximation

3. A standard single-phase simulation for flow dynamics and species transport is executed with the bubble being a prescribed and fixed domain boundary. The unstructured mesh employs surface-aligned cell-layers at the surface of the bubble.

The single-phase approach requires to recompute the steady flow field in the liquid phase. Based on the bubble rise velocity, an inflow velocity is applied at the outer domain boundary. Due to the absence of the gas phase, the interface velocity at the bubble-boundary must be modeled. A standard free-slip boundary condition may lead to qualitatively different flow fields compared to the two-phase flow simulation. Therefore, the interfacial velocity is mapped from the two-phase simulation to the single-phase simulation by means of machine learning. For more details on the implementation and the setup, the reader is referred to Sect. 3.3 in [8].

Once the flow field in the liquid phase is recomputed, transport equations for chemical species can be solved with excellent accuracy at low computational costs. At the bubble surface, a Dirichlet boundary condition for the transfer species is employed. For bulk or product species, a Neumann condition is applied. The current implementation does not account for the varying species concentration in the gas phase, which is a drawback compared to the two-scalar approach in FS3D. However, the main aim of the single-phase approach is the creation of high-fidelity reference data for the local and global mass transfer under complex conditions. Here, complex relates to the shape deformation, the flow field close to the bubble, or the mass transfer enhancement in the presence of chemical reactions.

3 Modeling of Convection-Dominated Concentration Boundary Layers

3.1 Overview

As outlined in the introduction, in a two-phase flow simulation it is hardly possible to place sufficient cells in the species concentration boundary layer. In the best case scenario, there is only a quantitative impact on the computed mass transfer performance. In scenarios where the species transport is tightly coupled with the flow dynamics [7, 11], more drastic side-effects occur. Results may be qualitatively wrong or the entire flow simulation may become unstable due to numerical problems in the solution of the species transport equations. Therefore, it is an essential step to understand the influence of low mesh resolution on the species transport. Once the main effects are isolated, subgrid-scale models can be designed to mitigate these effects. Here, two attempts to improve the species transport solution in the boundary layer are presented: the first one is based on analytical solutions of a simplified substitute problem, and the second one leverages highly resolved boundary layer data by means of machine learning. Both approaches are relatively easy to implement if the cells of the computational mesh are aligned with the interface. If the discrete interface is given by the PLIC elements in a Volume-of-Fluid simulation, the analytical profile functions are favorable, as detailed in Sect. 3.4.

3.2 Effect of Insufficient Mesh Resolution

Figure 4 depicts the first cell-layers of a mesh suitable for a finite-volume discretization of the liquid phase. The interface Σ separates the gas domain Ω^- from the liquid domain Ω^+. In gas-liquid systems, the high-Schmidt number problem is specific to the liquid phase because the Schmidt number in the gas phase is at least one order of magnitude smaller than in the liquid phase. Therefore, we focus only on the liquid phase in the explanations following hereafter. Important for further considerations are the cell-faces aligned with the interface, denoted by f_i^Σ, and the first layer of cell-faces normal to f_i^Σ, denoted by f_i^o ("opposite"). Moreover, it is assumed that the scalar fields for the species concentration are available in the cell-center of each control volume as values c_i.

In the numerical solution of a convection-diffusion equation using a finite volume discretization, the values and normal derivatives of a field have to be interpolated to the cell faces f_i to compute convective and diffusive fluxes. The species concentration field in a convection-dominated boundary layer is characterized by strong changes in direction normal to the interface. Therefore, the flux computation in interface normal direction is, in most cases, the one introducing the largest errors to the solution. The

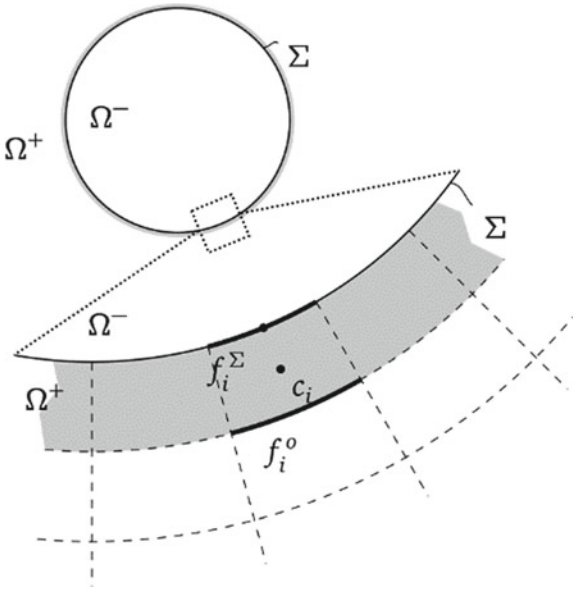

Fig. 4 Simplified 1D scenario to analyze the effect of low mesh resolution on convective and diffusive fluxes in the boundary layer

following explanations focus on the 1D scenario described before with x/δ_c being the normalized distance to Σ. A single reaction of type $2A + B \rightarrow P$ is considered, where A is the species being transferred from the gas to the liquid, B is a species present in the liquid bulk, and P is the formed product. This reaction is complex enough to explain also the main error sources in reactive species boundary layers with several parallel reactions involving additional species. It should also be noted that the reference concentration profiles, the cell averages and the interpolation lines in the following figures are computed from the numerical solution of boundary-value problems; see the footnotes in Chap. 5 of [8] for more details. The profiles are not artificially exaggerated but rather mitigated to allow a visual assessment.

Figure 5 focuses on the flux interpolation for the transfer species A. The typical normalized concentration profile $\tilde{c}_A$ corresponds to the solid blue line. In the scenario depicted in Fig. 5, the transfer species decays to zero within the first two cells. The numerical solution provides cell-centered values $\tilde{c}_{A,i}$ that correspond to profiles which are assumed to be constant within each control volume. In Fig. 5, the shaded blue areas correspond to the exact cell-averages in each cell computed from the solid-blue reference profile. Based on these values, the derivatives $d_x\tilde{c}_A(x/\delta_c = 0)$ and $d_x\tilde{c}_A(x/\delta_c = 0.5)$ as well as the concentration value $\tilde{c}_A(x/\delta_c = 0.5)$ have to be reconstructed (interpolated) in the first cell. A standard linear interpolation between the cell-centered values corresponds to the solid orange lines depicted in Fig. 5. Comparing the slope of the blue reference profile and the orange line segments clearly shows that the magnitude of the diffusive fluxes is underestimated at $x/\delta_c = 0$

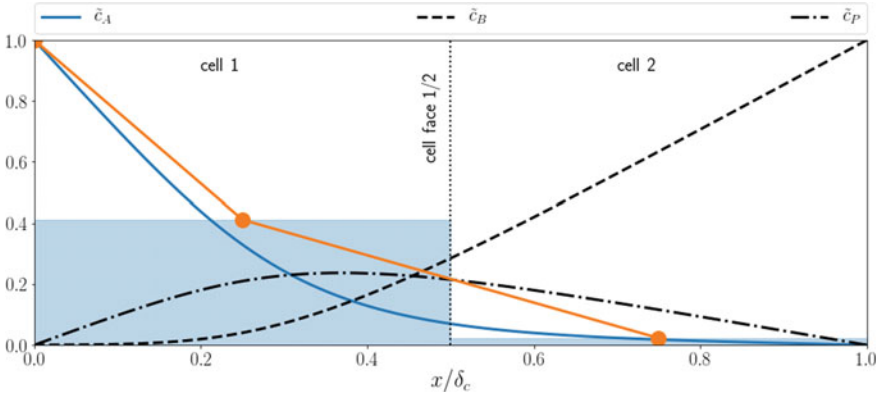

Fig. 5 Effect of low mesh resolution on convective and diffusive fluxes for the transfer species A

and over-predicted at $x/\delta_c = 0.5$. Considering the interpolated face value at $x/\delta_c = 0.5$, convective fluxes are strongly over-predicted. As the mesh gets refined, and more cells are located within the boundary layer, the interpolation error changes quantitatively and qualitatively. For this 1D scenario with exact cell-centered values, the interpolation error in the diffusive flux at $x/\delta_c = 0$ decreases monotonically with increasing resolution. The error in the diffusive flux at $x/\delta_c = 0.5$ is non-monotonous and changes sign. The interpolation error in the convective flux at $x/\delta_c = 0.5$ is also non-monotonous but does not change sign.[3]

All the aforementioned interpolation errors have a different weight in the resulting error of the species concentration field depending on the local Péclet number. Due to the complex changes of the individual error sources, the fact that even more error sources are present in the numerical solution of the full boundary layer problem, and the propagation of errors make it extremely difficult to provide a general estimate on how the resulting mass transfer is affected. However, the concentration boundary layer in 3D simulations of rising bubbles is typically so far below the necessary one that the global mass transfer is almost always underestimated. The same statement does not necessarily hold true for the local mass transfer.

The over- and underestimation of diffusive and convective fluxes also occurs for the bulk species B and the product species P. In many scenarios it is sensible to assume that the diffusive fluxes of both species is zero at the interface, meaning that neither B nor P is transferred to the gas phase or adsorbed onto the interface. Then the remaining error sources result from the interpolation at the first cell face normal to the interface. In contrast to the transfer species, even for the 1D example, errors in both diffusive and convective fluxes change non-monotonously, and the errors also change sign. For more information and visualizations, the reader is referred to Sect. 5.1 in [8].

[3] https://andreweiner.github.io/reveal.js/phd_defence.html#/3/2.

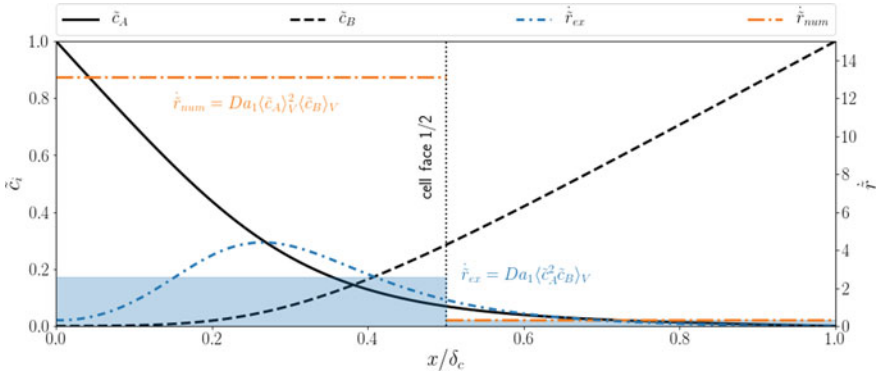

Fig. 6 Effect of low mesh resolution on the approximation of the reaction source term

Besides the fluxes, also reaction source terms introduce an error in case of insufficient mesh resolution. This effect has not been considered in the first data-driven implementation of the SGS model [10] because only a decay reaction was investigated. The effect depicted in Fig. 6 occurs if multiple educts are involved in a reaction. The effect is best described by the statement that the product of two averages is not necessarily equal to the average of the product. Computing the reaction source term in a single reaction from the cell-centered values $\tilde{c}_{A,i}$ and $\tilde{c}_{B,i}$ yields a much larger source term in the first cell compared to the one computed from the exact profiles. The effect is enhanced if the reaction order is higher, e.g., if two molecules of A are consumed in the reaction, and the overall reaction becomes third order.

Finally, it should be emphasized that all the error sources introduced in this section will influence one another, and it is difficult to predict the integrally observed effect on the concentration field. Moreover, for coupled reactions, the errors in one species concentration field influence the solution of all other species via the reaction source terms. Fortunately, the reference profiles depicted and analyzed in Figs. 5 and 6 can be approximated with high accuracy even if the boundary layer is completely embedded in a single cell layer. Non-linear profile reconstructions allow to compute improved flux estimates. The following section describes how physical profiles can be reconstructed based on analytical solutions and machine learning.

3.3 Analytical and Data-Driven Profile Reconstruction

Figure 7 shows the analytical solutions of a simplified substitute problem in case of physisorption and a first-order chemical reaction of the transfer species. These two-dimensional profiles have been used previously in subgrid-scale models for species transport in two-phase flows, and mathematical details on the substitute problem may be found in [5] for physisorption and in [6] for the reactive scenario. The mathematical expressions for both cases are depicted above each sub-figure. Useful approximate

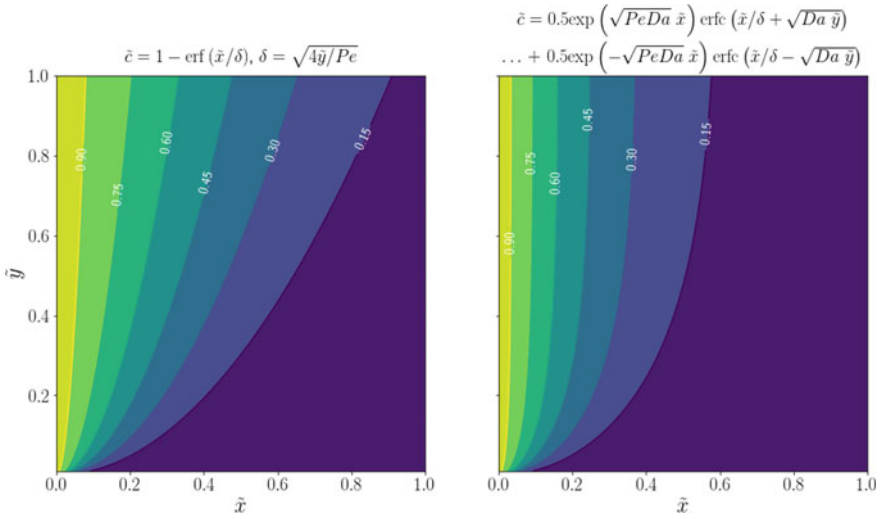

Fig. 7 Analytical solution of a simple substitute problem for physisorption (left) and a first order decay reaction (right)

profiles for the correction of numerical fluxes can be generated by evaluating the analytical solutions at a constant value of $\tilde{y}$. The resulting profile may be imagined as a slice through the concentration field in $\tilde{x}$-direction. The next logical step is to determine a sensible value for the unknown $\tilde{y}$.

Sensible approximations for $\tilde{y}$ may be found in two different ways outlined hereafter for physisorption. The known variables for each interfacial cell are the concentration at the liquid-side of the interface, the concentration in the cell center, and the cell geometry. To avoid round-off errors, the concentration profile of the transfer species is typically normalized with its interfacial value. In the simplified 1D scenario, the cell geometry may be reduced to the extension of the cell in interface normal direction and the position of the cell center. The cell-centered concentration can be interpreted in several ways, namely as the value of some concentration profile at the center or as the average concentration value in the cell. The latter interpretation is consistent with the formal definition of field values in a standard second-order finite volume discretization.

Figure 8 depicts the estimation of $\tilde{y}$ based on the interpretation that the cell-centered concentration value in the flow solver must be equal to the concentration value of the approximate profile function at the given distance from the interface. Note that for the special case of pure physisorption, it is more practical to adjust directly the parameter δ instead of $\tilde{y}$. In the example depicted in Fig. 8, the iteratively found fitting parameter is labelled as δ_{num}. If the model parameter is known, the reconstructed profile is suitable to compute improved numerical fluxes. In [5, 6], the concentration profile was used only to correct the diffusive flux at the interface. This fitting and correction scheme also appears in wall function modeling for turbulent flows or heat

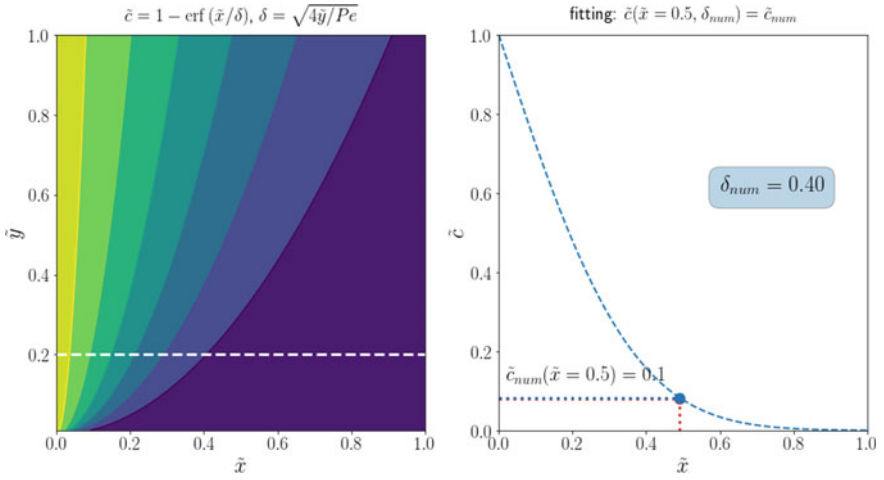

Fig. 8 Distance-based fitting of the model parameter for physisorption

transfer. Bothe and Fleckenstein [5] state that approximately one refinement level can be saved employing the non-linear flux correction at the interface, which results in a significant reduction of the mesh size, especially in 3D simulations. However, mass transfer simulations with physical Schmidt numbers require a saving factor of roughly 10–20.

Fortunately, the effectiveness of the profile reconstruction and flux correction can be significantly improved with a few small changes. The first modification, introduced in [9], is related to the profile reconstruction. Figure 9 visualizes how the model parameter δ_{num} is estimated based on the interpretation of the cell-centered concentration as the average cell value. The model parameter is iteratively adjusted until the integral of the approximate profile function over the cell volume is equal to the cell-centered value provided by the flow solver. Especially if the species transport equation is discretized explicitly in time, the integral fitting approach yields better flux approximations compared to the distance-based fitting because small errors in the numerical fluxes quickly lead to unphysical concentration over- and undershoots. The integral fitting condition significantly improves the connection between the amount of the species present in an interface cell and the amount of species leaving or entering the cell due to convective or diffusive fluxes. A second improvement introduced in [9] is a logical consequence of the error analysis in the previous section, namely that the reconstructed profile is also used to correct the convective and diffusive fluxes at all cell faces of each interfacial cell. The modified profile reconstruction and flux correction allows to approximate fully embedded boundary layers with astonishingly high accuracy. In [11], this approach was extended to account for a first-order reaction of the transfer species.

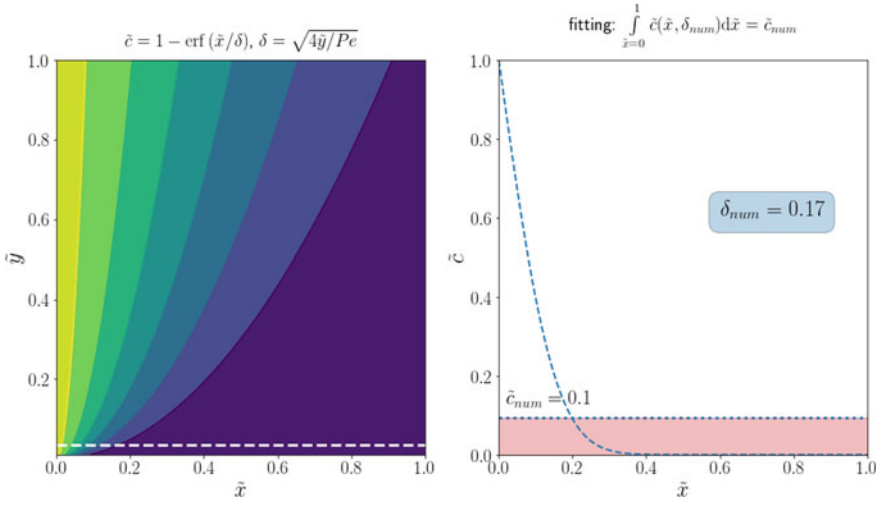

Fig. 9 Integral fitting of the model parameter for physisorption

Going beyond a single species and more complex or multiple reactions, the aforementioned approaches are limited by the availability of analytical profile functions. However, the numerical solution of moderately complex substitute problems, complex in terms of geometry and flow field, requires little effort and is practically not limited by the reaction type. A purely data-driven version of the subgrid-scale modeling approach described before would require the following steps:

1. Define a substitute problem that encompasses the main transport and reaction mechanisms and that can be solved with little computational effort.
2. Define model parameters characterizing the transport and reaction mechanisms, e.g., the Péclet and Damköhler numbers of all species.
3. Run a parameter variation of the substitute problem such that the target regime in the full simulation is included in the parameter space.
4. Extract the model parameters and the corresponding fluxes from the numerical data and employ them in the full simulation as replacement of the analytical solution.

The data extraction in the fourth step presumably requires some more detailed information and is therefore outlined in Fig. 10. A 1D species concentration profile in interface normal direction is considered. The mesh resolution in the numerical solution of the substitute problem should be high enough to place at least 10–20 cells within the boundary layer. Note that this value range is simply a rule of thumb. Fewer cells are possible if some loss in accuracy can be tolerated. More cells might be required if the concentration profiles are, for example, non-monotonous and have several extrema within the considered distance from the interface. The discretization scheme used to solve the substitute problem must be able to capture convective and diffusive fluxes, as well as the reaction sources terms with high accuracy. If this

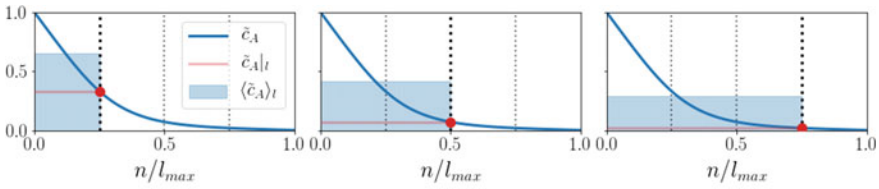

l/l_{max}	$\langle\tilde{c}_A\rangle_l$	$\tilde{c}_A\|_l$	...
0.25	0.65	0.32	...
0.50	0.41	0.07	...
0.75	0.29	0.02	...
...	...	...	...

Fig. 10 Feature extraction from the numerical solution of the substitute problem

criterion is fulfilled, one can now start to merge the cells in interface normal direction, one cell at a time, and compute how a well-resolved solution would look like on a coarser mesh. For example, considering the rightmost subfigure in the upper row of Fig. 10, the exact average concentration $\langle\tilde{c}_A\rangle_l$ of a single cell of length $l/l_{max} = 0.75$ can be computed by the volume-weighted average of the cell-centered concentration values in the first three cells. Moreover, the concentration at the first cell face of the extended cell $\tilde{c}_A(l/l_{max} = 0.75)$ can be approximated with high accuracy from the two neighboring cell-centered values. In the same way, the concentration normal derivative at the first cell face and at the interface can be computed. Following this procedure up to a sensible maximum distance l_{max} from the interface, one assembles input-target-value-pairs depicted in the table in Fig. 10.

An important step in the creation of data-driven SGS models is to decide which information should be extracted from the numerical solution of the substitute problem. An important criterion is that the model input data must be available in the target simulation. This requirement is more challenging to fulfill than it may seem on first sight. For example, the numerical solution of the substitute problem might be time-dependent and so is the full simulation. However, time is not a suitable candidate as model input. The transient behavior of both numerical solutions is most likely very different such that the concentration fields at the same time-instance are not comparable. This difference is by design since the substitute problem must be significantly simpler than the full problem. However, it is not necessarily true that there are no comparable states. The main challenge and maybe the art of SGS modeling is to find a small set of model inputs to map between similar states in both solutions.

A quite efficient feature to map results from the substitute to the full problem is the average concentration in interface normal direction. In the data-driven SGS modeling approach presented in [8, 10], it is identified as the feature explaining most of the variance in the numerical fluxes in convection-dominated concentration boundary layers. Due to the design of the substitute problem, the average concentration also

encompasses, to a large extend, effects like developing boundary layers, acceleration and deceleration as well as curvature effects. Note that it is still possible that additional model features may lead to an improved model performance.

The final question discussed in this section details how the discrete input-target-value-pairs might be employed in the full simulation. If the gathered data are relatively small, the simplest approach is to interpolate fluxes between the K nearest neighbors in the input space. However, as the data size increases, such non-parametrical approaches become less and less practical since many search operations have to be performed. Instead, in [8, 10] we used multilayer-perceptrons (MLP) to create approximate functions based on the extracted data. MLPs are characterized by high parameter efficiency. For example, in [10] a model with only 230 parameters was sufficient to approximate about two million training data points.

3.4 Implementation in Simulation Approaches

The SGS modeling approaches outlined in the previous section have been implemented and tested in several different two-phase and single-phase flow solvers. The implementation in a geometrical Volume-of-Fluid approach is the most effortful one and was only performed based on the analytical profile functions. In contrast to the explanations in the previous section, the reconstructed interface is typically not aligned with the surrounding cell faces. The concentration profile in each interface cell is still considered to be 1D in interface normal direction, but the integral fitting as well as the flux computation require the solution of complex volume and surface integrals. In Fig. 11, the reconstructed plane segment splits the cubic volume cell

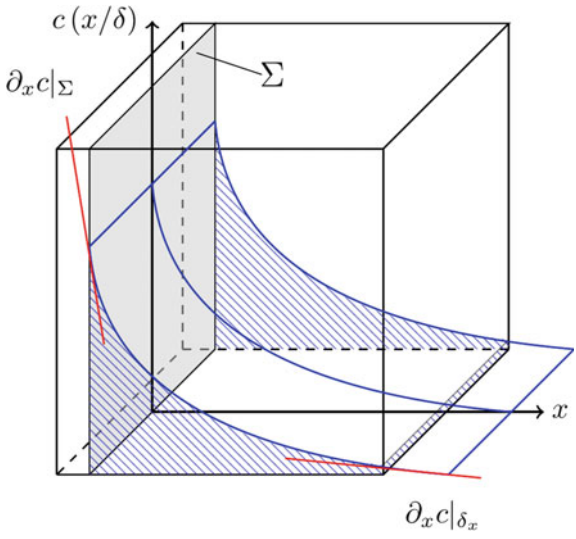

Fig. 11 Cartesian background mesh cell with reconstructed interface and embedded concentration profile normal to the interface

into two sub-cells representing the two phases. The profile function has to be integrated over the remaining volume, representing the liquid phase, to find the model parameter via the integral fitting approach. Once the model parameter is determined, the face average of each flux-term over each face of the liquid phase volume has to be computed. In [9], both volume and surface integrals were evaluated analytically for pure physisorption. Even for a simply decay reaction, the analytical evaluation is no longer practical, and numerical integration would be necessary. If numerical integration is available, it is also possible to employ the data-driven modeling approach in the Volume-of-Fluid context.

The SGS model has been also implemented in an Interface-Tracking approach [7, 11] and in a single-phase solver [8], with the latter case serving mainly for validation. Both implementations are very similar in nature and are therefore outlined jointly hereafter. The implementation requires that the mesh has at least one interface-aligned cell-layer. In contrast to the Volume-of-Fluid approach, the time-discretization is implicit. Therefore, the flux-terms cannot be overwritten directly with SGS information coming from the analytical profile or approximate functions. Instead, the molecular diffusivity coefficient and the face-velocity are adjusted based on the ratio of SGS-prediction to standard discretization. For example, if the standard discretization underestimates the diffusive flux at the interface, then the diffusivity coefficient is artificially increased at these faces. This correction approach is also applied in wall function models in the field of turbulence modeling. For more detailed information, the reader is referred to the literature [7, 8].

3.5 Validation

This section presents only a small excerpt of the extensive validation in [9] for the Volume-of-Fluid implementation, in [7, 11] for the implementation in Interface-Tracking based on analytical profile functions, and in [8, 10] for the data-driven approach. The difficulty in validating the various SGS-model flavors lies in the absence of high-fidelity reference data. Experimental data are only available in the form of integral mass transfer coefficients. Moreover, even for simple cases, the 95% confidence interval can easily be about 50% of the computed mean value [11] and, hence, such data is not suitable to validate a numerical method, where the relative improvement due to the modeling is in the same range. It has been also shown that the local Sherwood number might be sometimes over- and sometimes underestimated as a consequence of insufficient mesh resolution [8]. Consequently, global mass transfer quantities may appear more accurate due to a favorable compensation of different error sources. Therefore, local and global quantities should be compared against reference data. Such reference data can be obtained using semi-analytical approaches. In [5, 6, 9], the analytical flow field solution for a spherical particle rising in Stokes-flow was used to obtain a highly resolved numerical solution of the concentration field in the species boundary layer. This approach provides local and global reference data of high quality. A drawback is that shape and flow field

are not very representative for the highly chaotic regimes encountered in bubble swarms at high Reynolds numbers. Hence, it is difficult to assess how well a model will perform in such complex circumstances. As a step towards more realistic reference data, the hybrid approach outlined in Sect. 2.2 was developed. Currently, the hybrid approach allows to create reference data for the steady rise of highly deformed bubbles with complex flow fields. The extension to dynamic scenarios is planned for future developments.

Based on the hybrid simulation approach, the data-driven SGS models have been assessed for several reaction mechanisms, with the most complex reaction being a parallel-consecutive reaction involving four different species. Important criteria for data-driven SGS models are the ability to generalize to various flow scenarios and an independence of the model performance from the underlying mesh resolution. In both categories, the data-driven SGS model performs approximately as well as the versions based on analytical profile functions for physisorption. Even for complex reactions with multiple species, the deviation in terms of global Sherwood number typically ranges between one and four percent [8, 10]. An analysis of the local Sherwood numbers shows that there is some space for further improvements in regions of high species concentrations close to the interface, for example, in the presence of recirculation zones and flow detachment. Additional model features could help to improve the model's accuracy in these regions.

4 Reactive Species Transport Around Single Rising Bubbles

4.1 Overview

The single-phase approach introduced in Sect. 1.2 was originally developed to create highly realistic reference data to validate SGS modeling approaches. A positive side-effect is that the generated concentration fields allow detailed insights into the species transport around highly deformed bubbles. Such data are typically not accessible by experimental means, and numerical results obtained with two-phase flow solvers are little insightful due to insufficient mesh resolution or unphysical simulation parameters. This section presents an excerpt of the results obtained with the hybrid approach in terms of concentration fields, local and global mass transfer parameters, and local selectivity fields for a parallel-consecutive reaction.

4.2 Velocity and Concentration Fields

Based on the hybrid approach, the steady species transport around bubbles of various shapes has been investigated in [8]. Three of the more exotic rise behaviors are depicted in Fig. 12. The figure visualizes the full two-phase flow field computed

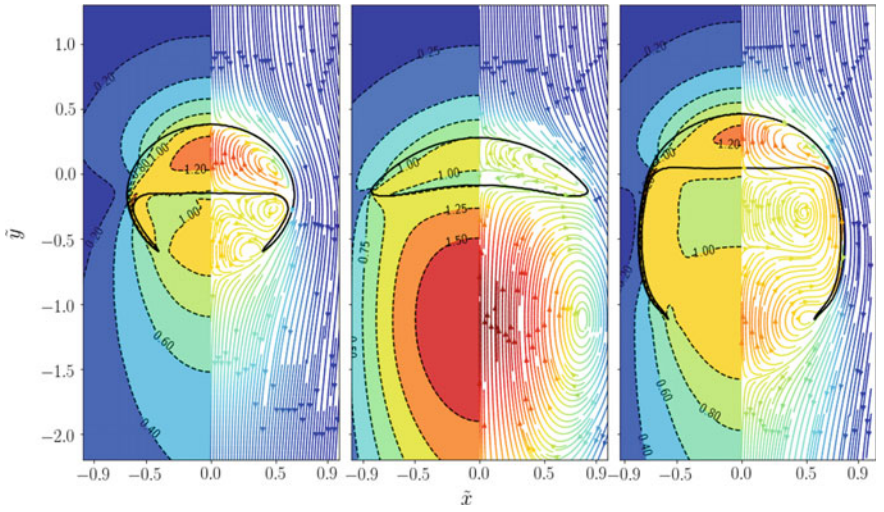

Fig. 12 Velocity field around dimpled ellipsoidal, spherical cap, and skirted bubbles (from left to right) visualized as contour plot of the velocity's magnitude and as streamline plot colored by the magnitude. For the exact simulation settings in terms of Morton, Eötvös, and Galilei number, refer to Table 6 in [8]

using the Basilisk flow solver introduced in Sect. 2.1. The two-phase flow field is a required input for the single-phase solver because the gas phase is omitted and sensible boundary conditions for velocity and pressure at the bubble-boundary of the single-phase domain must be derived. The examples in Fig. 12 have been selected because several recirculation zones appear despite the steadiness of the rise. When employing a free-slip boundary condition at the bubble surface instead of a data-driven boundary condition based on the two-phase flow solution, these flow patterns will not appear in the same form; see Sect. 6.4.2 in [8] for a visualization. Especially the dimpled-ellipsoidal and skirted bubbles contain recirculation zones in the rear part of the bubble that keep a portion of the liquid bulk trapped. From the point of view of reaction engineering, these zones are of interest because reaction products and transfer species accumulate, while bulk-species become slowly depleted. Therefore, such shape regimes might be favorable or unfavorable towards the formation of products or side-products. Consequently, it is essential to have a single-phase flow field that resembles its two-phase counterpart as closely as possible.

Also for relatively simple cases in which the flow field around the rising bubble is closed, a standard free-slip boundary condition for the velocity introduces a significant quantitative error even though the flow field is qualitatively correct. Figure 13 compares the velocity fields obtained with the data-driven and the free-slip boundary condition against the two-phase flow field. There is an obvious discrepancy in the wake velocity obtained with the free-slip boundary condition. This difference results

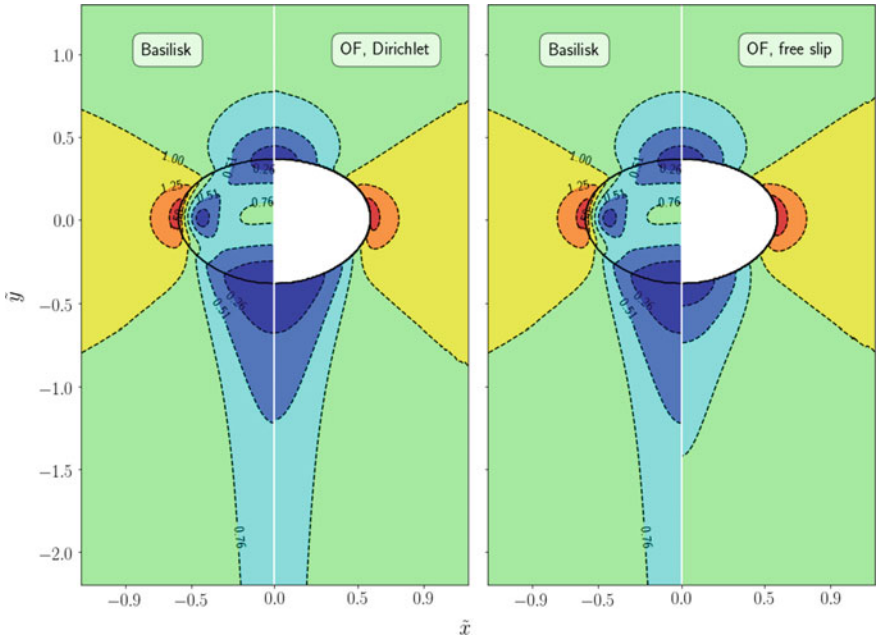

Fig. 13 Comparison of the velocity fields obtained with two-phase and single-phase simulation approaches

from the shear stresses introduced by the gas phase that is by definition zero when employing a free-slip boundary condition. There is also a subtle difference in the velocity field close to the bubble surface. As will be shown in Sect. 4.3, such a small deviation in the velocity boundary layer is enough to cause a difference larger than 5% in the computed mass transfer. On the other hand, the data-driven boundary condition results in a velocity field that is almost indistinguishable from the two-phase flow solution. Since the species transport is modeled as a passive process in the results presented hereafter, it is assumed that concentration field and mass transfer properties computed with the hybrid approach reflect the true two-phase species transport solution more closely than single-phase simulations employing a free-slip boundary condition.

Figure 14 depicts exemplary species concentration fields for a parallel-consecutive reaction occurring around a dimpled ellipsoidal bubble. An advantage of the single-phase simulation is that extremely dense meshes can be created such that it is possible to use realistic values for the molecular species diffusivities. Unfortunately, the resulting concentration boundary layers are so thin that they are hardly observable in images. This observation emphasizes the need for complementary numerical simulations since a visual inspection of the boundary layer by experimental means is currently not feasible.

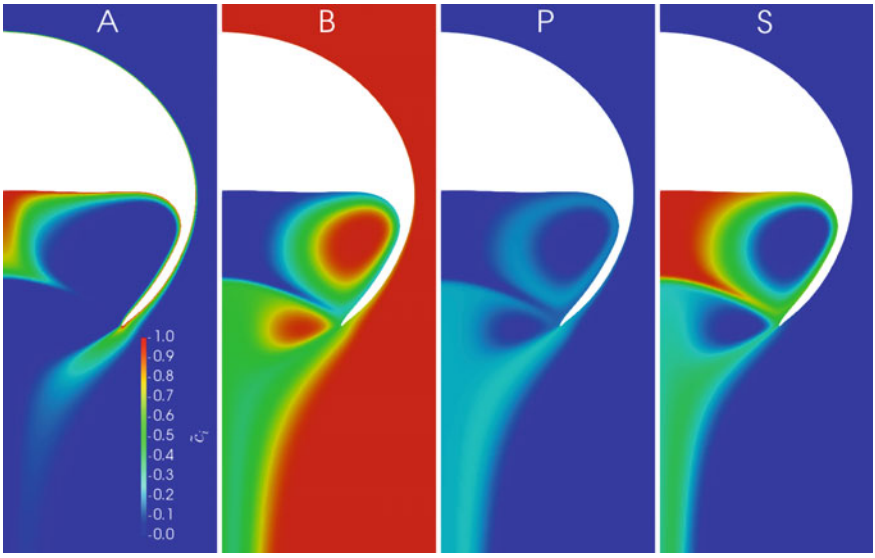

Fig. 14 Concentration fields around a dimpled ellipsoidal bubble in case of a competitive-consecutive reaction (A + B → P and A + P → S)

The liquid portion in Fig. 14 enclosed by the bubble's tail presents an interesting example for the interplay of different transport and reaction mechanisms. The transfer species *A* reacts with the bulk species *B* and forms the product *P*. Since the diffusive transport from the surrounding liquid bulk into the entrapped liquid portion is slower than its consumption by the chemical reaction, a significant depletion of *B* occurs close to the center line. At the same time, the consumption of *A* in this region drops due to the absence of *B*, and *A* accumulates. The presence of both species *A* and *P* in the entrapped liquid portion increases the formation of the side product *S*. The side product accumulates in the wake region. Note that the naming convention of product and side product is rather arbitrary. If *S* was the desired product, then the dimpled ellipsoidal bubble itself would be a favorable "micro-reactor". An additional analysis of the product formation, also for other bubble shapes, follows in Sect. 4.4.

4.3 Species Transfer and Enhancement

The global Sherwood number and the enhancement factor are the two most important quantities for scale-reduced modeling of reactive mass transfer processes. The Sherwood number *Sh* is a dimensionless version of the mass transfer coefficient k_L defined as:

$$Sh_{\text{eff}} = \frac{k_L d_{eq}}{D} \text{ with } k_L = \frac{\dot{n}}{A_{\text{eff}} \Delta c}. \tag{3}$$

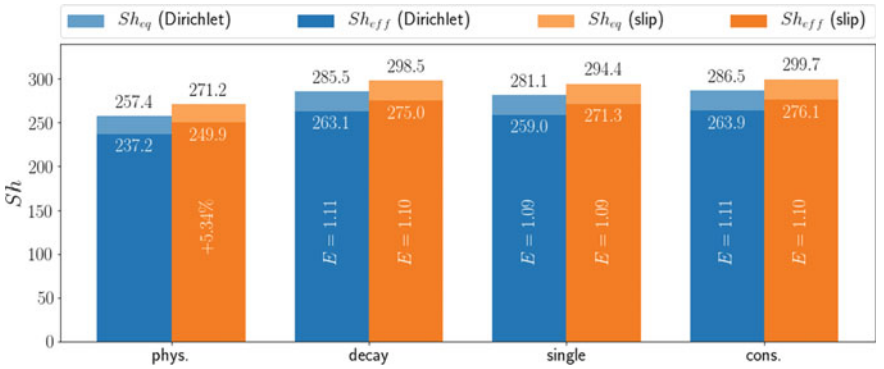

Fig. 15 Global Sherwood number and enhancement factor for a $d_b = 1.8$ mm air bubble rising in water

The effective surface area A_{eff} is often not known and not explicitly computed in experimental investigations. Instead, the bubble volume is measured, and volume-equivalent diameter d_{eq} and surface area A_{eq} are used to compute *Sh*. These different definitions are important to keep in mind when comparing the mass transfer at non-spherical bubbles between simulations and experiments or literature correlations. Both *Sh*-relations are connected to one another by the ratio of equivalent to effective surface area:

$$\frac{Sh_{\text{eff}}}{Sh_{eq}} = \frac{A_{eq}}{A_{\text{eff}}}. \tag{4}$$

Figure 15 depicts the global Sherwood numbers at a small air bubble rising in water. The investigated reaction mechanisms are as follows:

Label	Reaction
Decay	$A \rightarrow P$
Single	$A + B \rightarrow P$
Consecutive (cons.)	$A + B \rightarrow P \,\&\, A + P \rightarrow S$

Figure 15 depicts both effective and equivalent Sherwood number. From their ratio, the increase of the surface area due to the interface deformation can be inferred. Noticeably, even for the simplest investigated case with a closed flow around the bubble, employing a free-slip boundary condition for the velocity at the bubble surface leads to a five percent higher prediction of the mass transfer. In contrast, the computed enhancement factors remain mostly unaffected.

Visualization 16 depicts equivalent information as Fig. 15 but for the dimpled ellipsoidal bubble analyzed in previous sections. A striking difference is the more than two times enlarged effective surface area. Due to the complex flow field, which is not reproduced well employing a free-slip boundary condition, also the discrepancy

between the two different velocity boundary conditions increases. A difference of roughly 30 percent manifests for the Sherwood number and the deviation of the enhancement factor ranges between 9% and 13% (Fig. 16).

A strong side of numerical simulations is the availability of local information close to the gas-liquid interface. For example, one may analyze the local Sherwood number Sh_{loc} to understand the behavior of the global Sherwood number in different flow regimes or reaction systems. Figure 17 depicts the local Sherwood number at a dimpled ellipsoidal bubble for different reaction types. Plots depicting the local Sherwood number over the polar angle φ for axis-symmetric bubble shapes are common in literature. However, the curves depicted in Fig. 17 require some more explanation. In contrast to spherical or ellipsoidal bubbles, the surface of a dimpled ellipsoidal bubble does not form a convex hull. However, it is still possible to analyze

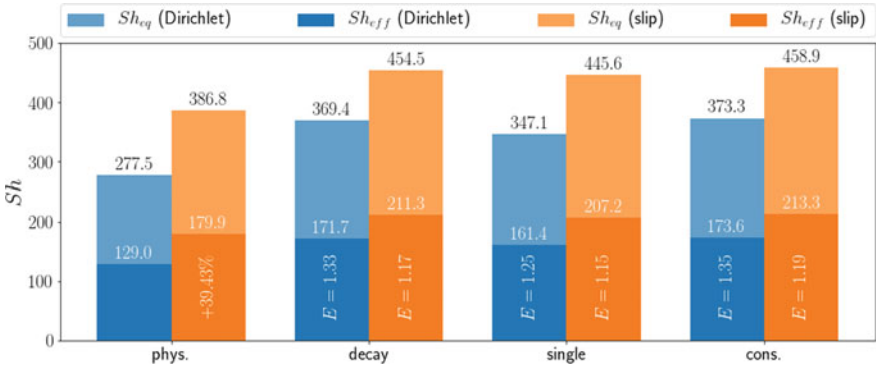

Fig. 16 Global Sherwood number and enhancement factor for a dimpled ellipsoidal bubble

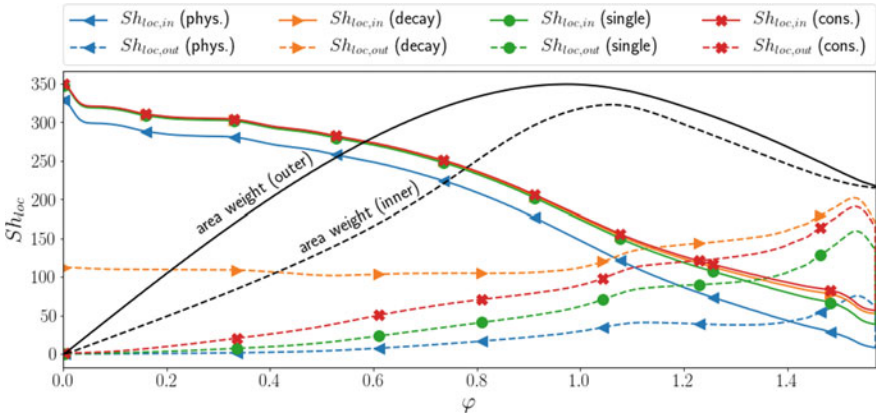

Fig. 17 Local Sherwood number for a dimpled ellipsoidal bubble. The area weight indicates to which extend the local Sherwood number at a given polar angle contributes to the global Sherwood number

the mass transfer with respect to the polar angle, but for each polar angle two local Sherwood numbers are available, one for the inner and one for the outer contour. Moreover, it helps for the interpretation of the influence on the global Sherwood number to know the contribution (weight) of the local Sherwood number to its global counterpart. The weight is nothing but a normalized version of the circumference at a given point on the interface. As for the local Sherwood number, there are two weighting factors for each polar angle.

On the outer contour of the dimpled ellipsoidal bubble, the mass transfer is qualitatively similar for all reaction types. On the inner contour, the picture changes drastically. In case of physisorption, the mass transfer drops to almost zero due to the accumulation of the transfer species in the entrapped liquid volume. Consequently, the presence of a chemical reaction leads to a relatively strong enhancement at the inner contour of the bubble. For a simple decay reaction, the enhancement is mostly uniform with respect to the polar angle. In contrast, the enhancement for single and parallel consecutive reactions decreases to zero close to the center line because of the strong depletion of bulk species in that region.

4.4 Local Selectivity

A quantity of high interest for chemical engineers is selectivity. While it is ultimately important to know how much product and side product are formed integrally, the local selectivity depicted in Figs. 18 and 19 reveals regions where product or side product are mainly formed. We define the local selectivity for a parallel-consecutive reaction as

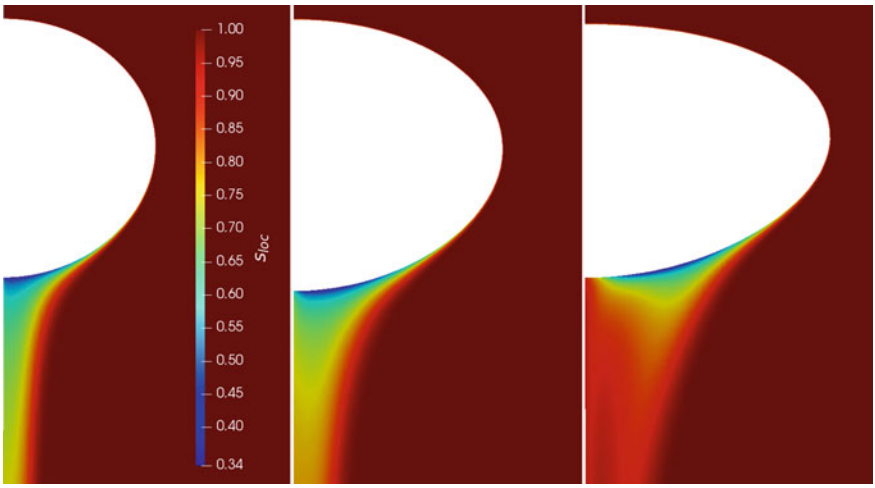

Fig. 18 Local selectivity around small ellipsoidal bubbles with increasing aspect ratio from left to right

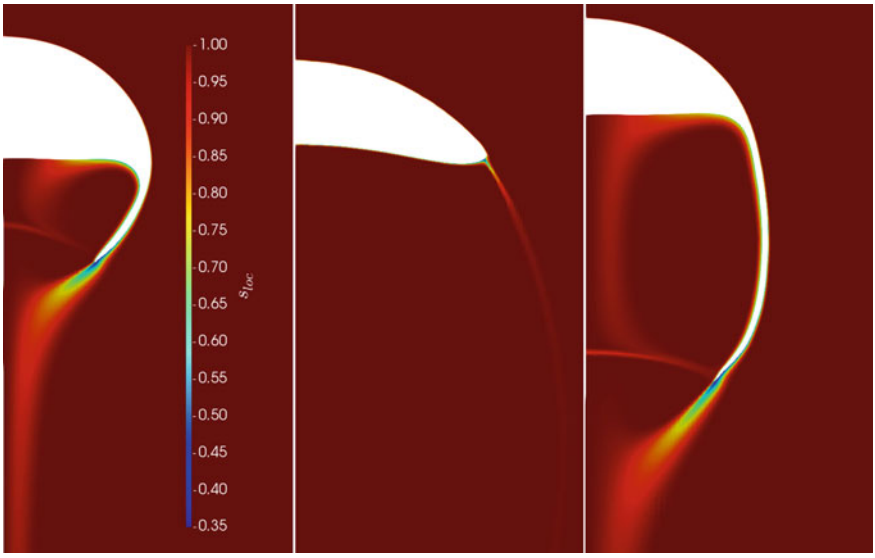

Fig. 19 Local selectivity around dimpled ellipsoidal, spherical cap, and skirted bubbles (from left to right)

$$s_{loc} = \frac{r_1 - r_2}{r_1 + r_2}, \tag{5}$$

where r_1 and r_2 are the reaction source terms for the first and second reaction, respectively. Following the naming scheme from before, the source terms are computed as $r_1 = k_1 c_A c_B$ and $r_2 = k_2 c_A c_P$ with the reaction rate constants k_i. Note that there are several sensible definitions for the local selectivity. A disadvantage of the definition above is that integrating s_{loc} over the fluid domain does not yield the global selectivity. However, an advantage is that the fields in Figs. 18 and 19 are not masked by other transport mechanisms.

Figure 18 shows the local selectivity in the wake of ellipsoidal bubbles for three different aspect ratios. Such ellipsoidal bubbles occur, for example, if small air bubbles rise in uncontaminated water at room temperature. The increasing aspect ratio and Reynolds number reflects an increase in the bubble volume. Regions of low selectivity towards the primary product occur in the rear part of the bubbles. As the aspect ratio increases, the point of lowest selectivity shifts from the pole towards the equator. Moreover, there is a tube-like region of low selectivity in the wake of the almost spherical bubble. As the aspect ratio increases, this region becomes shorter. Note that it is not straightforward to judge from these observations which bubble size might be favorable to maximize the global selectivity. However, Fig. 18 may help to identify the various effects that lead to a change in the global selectivity.

The local selectivity fields in Fig. 19 are much more diverse compared to the ones in Fig. 18. Comparing Figs. 14 and 19, one observes that regions of low selectivity in the entrapped liquid volume coincide with regions of high product accumulation for

the dimpled ellipsoidal bubble. Another region of low selectivity forms around the tail of the bubble's skirt. The skirted bubble shows a similar behavior. Interestingly, only a very small region of low selectivity forms around the spherical cap bubble. This region coincides with the point (or ring), where the flow detaches from the interface. Due to the enormous size of the recirculation zone behind the spherical cap bubble, no significant depletion of the bulk species occurs, which is in contrast to the other bubble shapes analyzed here.

5 Conclusion and Outlook

In this chapter we presented new modeling techniques to investigate the reactive mass transfer at rising bubbles. Regarding the high-Schmidt number problem, a subgrid-scale modeling approach was described that allows to approximate species concentration boundary layers with high accuracy even if they are fully embedded in a single cell layer around the gas-liquid interface. This modeling approach may be used in the future to investigate the reactive mass transfer in bubble swarms. Numerical simulations of bubble swarms allow to investigate their chaotic behavior, and the subgrid-scale model may aid to compensate the decreased mesh resolution per bubble diameter, which would be insufficient to resolve the species boundary layers for realistic Schmidt numbers. To validate the SGS model performance, a hybrid simulation approach was developed that maps the two-phase interfacial velocity onto a single-phase simulation domain based on machine learning. The hybrid approach also allows to take a close look at the local species transport around various typical bubble shapes.

For future investigations it is desirable to investigate the data-driven version of the SGS model in greater detail than presented here and in [8, 10]. Regarding the hybrid approach, a version of the tool *snappyHexMesh* optimized for two-dimensional meshes would greatly simplify the creation of meshes that are dense enough to resolve the extremely thin species concentration boundary layers. Moreover, the potential of the hybrid approach should be exploited to create high-fidelity reference data for the reactive mass transfer at realistic bubble shapes. Such data can be used in consecutive steps to create more accurate Sherwood number and enhancement factor correlations and to validate the SGS model performance under more realistic and challenging conditions.

Acknowledgements This work was funded by the Deutsche Forschungsgemeinschaft (DFG, German Research Foundation)—priority program SPP1740 "Reactive Bubbly Flows" (237189010) for the project BO 1879/13-2 (237189010).

References

1. Levich VG (1962) Physicochemical hydrodynamics. Prentice Hall, Upper Saddle River
2. Aboulhasanzadeh B, Hosoda S, Tomiyama A, Tryggvason G (2013) A validation of an embedded analytical description approach for the computations of high Schmidt number mass transfer from bubbles in liquids. Chem Eng Sci 101:165–174
3. Aboulhasanzadeh B, Thomas S, Taeibi-Rahni M, Tryggvason G (2012) Multiscale computations of mass transfer from buoyant bubbles. Chem Eng Sci 75:456–467
4. Claassen CMY, Islam S, Peters EAJF, Deen NG, Kuipers JAM, Baltussen MW (2020) An improved subgrid scale model for front-tracking based simulations of mass transfer from bubbles. AIChE J 66(4):e16889
5. Bothe D, Fleckenstein S (2013) A volume-of-fluid based method for mass transfer processes at fluid particles. Chem Eng Sci 101:283–302
6. Gründing D, Fleckenstein S, Bothe D (2016) A subgrid-scale model for reactive concentration boundary layers for 3D mass transfer simulations with deformable fluid interfaces. Int J Heat Mass Transf 101:476–487
7. Pesci C, Weiner A, Marschall H, Bothe D (2018) Computational analysis of a single rising bubble influenced by soluble surfactant. J Fluid Mech 856:709–763
8. Weiner A (2020) Modelling and simulation of convection-dominated species transport at rising bubbles. PhD thesis, Technical University of Darmstadt, Darmstadt, Germany
9. Weiner A, Bothe D (2017) Advanced subgrid-scale modeling for convection-dominated species transport at fluid interfaces with application to mass transfer from rising bubbles. J Comput Phys 347(1):261–289
10. Weiner A, Hillenbrand D, Marschall H, Bothe D (2019) Data-driven subgrid-scale modeling for convection-dominated concentration boundary layers. Chem Eng Technol 42(7):1349–1356
11. Weiner A, Timmermann J, Pesci C, Crewe J, Hoffmann M, Schlüter M, Bothe D (2019) Experimental and numerical investigations of reactive species transport around a small rising bubble. Chem Eng Sci X 1:100007